L.S. MAKSIMENKO, I.E. MATYASH, O.N. MISCHUK, S.P. RUDENKO,
B.K. SERDEGA, M.A. STETSENKO

V.E. Lashkaryov Institute of Semiconductor Physics, Nat. Acad. of Sci. of Ukraine
(41, Nauky Ave., Kyiv 03028, Ukraine; e-mail: bserdega@gmail.com)

PACS 73.20.Mf

SPECTRAL ANALYSIS OF POLARIZATION CHARACTERISTICS OF SURFACE PLASMON RESONANCE IN NANOSIZED GOLD FILM

Polarization properties of the surface plasmon resonance (SPR) in a nanosized gold film fabricated by the thermal evaporation are studied with the use of the internal reflection method and the modulation polarimetry technique. The spectral and angular characteristics of the reflection coefficients for linearly polarized radiation at fixed azimuths of the electromagnetic wave field directed in parallel, R_p^2, and perpendicularly, R_s^2, to the incidence plane are measured, as well as those of the polarization difference $\rho = R_s^2 - R_p^2$, which is a product of the modulation technique. A well-pronounced asymmetry of the $\rho(\lambda)$ spectra is revealed. A method of determination of the non-resonant component in the $\rho(\lambda)$ spectra is developed, and the approximation of spectra by Gaussian functions with regard for this asymmetry is done. Three resonant components are resolved in the resulting characteristics $\rho_{\mathrm{SPR}}(\lambda)$, and their interpretation based on the previously developed theoretical model of waveguide modes at both film surfaces is proposed. The parameters of resonances are determined, and the corresponding dispersion relations are plotted.

K e y w o r d s: modulation polarimetry, surface plasmon resonance, waveguide modes, dispersion.

1. Introduction

A lot of earlier [1–5] and modern [6] books, a large number of scientific reviews [7–10], and a huge number of journal publications are devoted to the consideration of the surface plasmon resonance (SPR) in nanosized metal films. Such attention is a result of a deep physical content of this phenomenon characterized by a variety of properties and a wide scope of applications [11]. In view of the popularity of SPR phenomenon for a long time and the perfection of its study, all relevant unrevealed issues should seemingly have been resolved; at least those concerning its manifestations in homogeneous media. However,

modern solid state nanophysics deals with plenty of composite materials [12], the conductivity of which is sufficient for the SPR to emerge. In addition, combinations of various metal components in the form of clusters in composite films and matrix materials generate an almost inexhaustible set of relations between their optical constants and, as a consequence, an almost inexhaustible variety of films with different dielectric properties. Their testing using atomic-force microscopy (AFM), the method that is deservedly widespread in nanomaterials science, becomes problematic, because the contact reconstruction of the internal surface and, hence, the form of clusters is impossible. A necessity in this information is associated with the problem of creating new composite materials, the electrodynamic properties of which are driven by indicated factors in the form of various dimen-

sional effects. The establishment of regularities in the degree of mutual influence of the matrix parameters and the cluster nature with regard for the dimensions, shapes, and spatial orientations of clusters, as well as their volume fraction in the material and how this fraction affects the end-product properties, is a challenging problem. The results of its solution will form a basis for the development of new materials and the prediction of their properties.

The way to tackle this task should consist in studying the evolution of optical characteristics, determining the corresponding constants, and establishing their relation to the degree of material dispersion in the course of the controllable morphological transition from a continuous homogeneous metal film to a composite one. Concerning the methods aimed at studying the surface topology, the transmission electron microscopy (TEM) can be, to some extent, an alternative to the AFM. However, the both are only auxiliary techniques and cannot pretend functionally to determine the electrophysical properties of examined objects. At the same time, the development of nanomaterials science needs in a method that would be informative at studying the cluster materials from the viewpoint of both the morphology of investigated objects and their electrodynamic properties.

That is why the spectroscopy of the total internal reflection violated by a resonance-sensitive film on the prism surface attracts a special interest. The foundation for such attention is formed by a "powerful" measurement and analytical method based on the modulation polarimetry (MP) technique. After the first publication [13], its fruitfulness was demonstrated in a series of papers, which were generalized in work [14]. In this work, we develop the information capability of MP further with the use of the simplest example, namely, the systematization of polarization properties of a nano-sized homogeneous gold film, the thickness of which is optimal from the viewpoint of the SPR emergence.

2. Experimental Technique and Measurement Results

The details of the MP technique were explained in work [15]. Its role in measurements consists in the resolution of medium's response to the actions of the polarized and almost always available non-polarized radiation components. The latter, being not related to the anisotropic properties of material, is a factor that restricts the detection ability of the measuring systems with respect to anisotropy effects. This factor can be avoided taking advantage of the property of the polarized radiation component, in contrast to the non-polarized one, to response to the action of the polarization modulation. In this case, a photodetector transforms the modulated radiation component into a varying signal, which can be separated from the non-polarized component with the use of a selective amplifier. In the first place, this operation enhances the detection ability of the MP-based measurement systems by orders of magnitude. In addition, the polarization origin of the measured result becomes more substantiated.

The analytical role of the MP technique consists, first, in its ability of resolve elliptically (in the general case) polarized radiation into the circularly and linearly polarized components; and, second, in that one of the linear components of polarized radiation, which in the representation of the Stokes vector component corresponds to the relation $Q = E_x^2 - E_y^2$ [16], where E_x^2 and E_y^2 are the radiation intensities of orthogonal wave components, presents a possibility of the functional analysis. The meaning of the Q-component consists in that the general features of functions in this relation – or any other analyzed effect (optical, photo-electric, magneto-optical, and other) – disappear at their subtraction. The remaining result contains the specific features of either of terms and, owing to the amplification, provides, first of all, an ultrahigh sensitivity of the system to the variations in the polarization state or the physical factors that are responsible for this effect. In addition, as a component (numerator) of the expression that determines the mathematical derivative of the corresponding function, the result of subtraction under the condition $Q \ll \left(E_x^2, E_y^2 \right)$ really reminds, by its form, a derivative with respect to the corresponding argument obtained by physical differentiation.

The research installation consisting of a goniometer connected to a monochromator allowed the angular polarization characteristics of internal reflection parameters to be measured at various wavelengths λ, or their spectral characteristics at definite radiation incidence angles θ. According to the reasons given above, the characteristics of the polarization difference $\rho(\lambda, \theta) = R_s^2 - R_p^2$ between the internal reflection coefficients, when the azimuth of the electric field

in the incident wave periodically changes perpendicularly, $R_s^2(\lambda, \theta)$, and in parallel, $R_p^2(\lambda, \theta)$, to the incidence plane, were the aim of our measurements. We should emphasize that the result of a physical subtraction is free of errors that accompany this operation in the mathematical procedure dealing with the results obtained at consecutive measurements. If necessary, the dependences of the coefficients $R_s^2(\lambda, \theta)$ and $R_p^2(\lambda, \theta)$ could be measured separately and used as auxiliary ones while analyzing the spectra. The measurements were carried with the help of a lock-in nanovoltmeter, in which the phase of the reference signal was established to provide the positive sign for the parameter $\rho(\lambda, \theta)$, which corresponds to the condition of normal internal reflection ($R_s^2 > R_p^2$).

The technical parameters of the measurement installation were as follows. A helium-neon laser with a wavelength of 0.632 μm played the role of a source of monochromatic polarized radiation, whereas a diffraction monochromator equipped with a halogen tube and a polarizer was used as a radiation source with the spectrum within the interval 0.4–1 μm. A dynamic phase plate [17] with a modulation frequency of 50 kHz played the role of a modulator, and a silicon photodiode did the role of a photodetector.

Gold films (99.999% of Au) were fabricated by the thermal evaporation of the metal in vacuum from a molybdenic heater (1×10^{-5} mm Hg) onto fused quartz substrates held at room temperature. The rate of gold film sputtering amounted to about 1.5 nm/s, and the film thickness was determined with the use of a calibrated quartz resonator and equaled 50 nm. Substrates 1 mm in thickness being in contact through an immersion liquid with a corresponding segment fabricated from the same material compose a semicylinder.

The results of measurements of the parameter $\rho(\lambda)$ at various incidence angles from the interval below the critical value are depicted in Fig. 1 in the coordinates determined by the conditions of the experimental installation. The angle values were so selected that the dispersion of the function $R_p^2(\theta)$ was the strongest, which is the main attribute of the SPR phenomenon and, as a consequence, the origin of the observed evolution of the spectrum $\rho(\lambda)$. Really, in the studied wavelength interval 400 nm $< \lambda <$ 1000 nm, the profiles of all presented characteristics are typical of resonance phenomena. Moreover, all the curves demonstrate a common tendency to coincide beyond
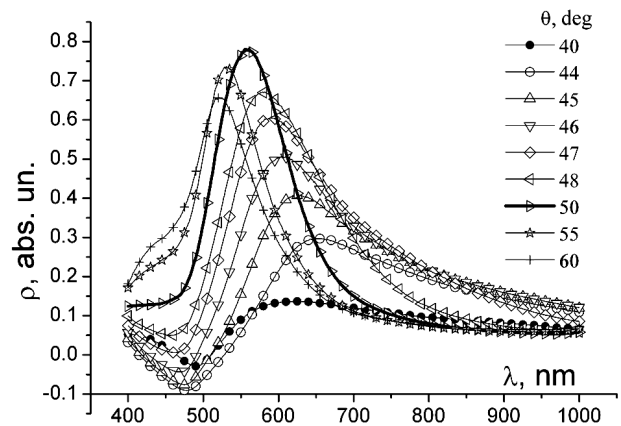

Fig. 1. Evolution of the $\rho_\theta(\lambda)$-spectra for an Au film with $d = 50$ nm associated with the variation of the light incidence angle

the indicated wavelength range, which testifies to the parameter independence of the incidence angle, i.e. $\rho \neq f(\theta)$. Since the resonant interaction is absent beyond this wavelength interval and the parameter $\rho(\lambda)$ always has a certain non-zero value, there is no doubt that the non-resonant component of the reflection coefficients is also present within the indicated limits. However, the most important is the fact that all characteristics contain attributes (more or less pronounced) of one more component that may be of the resonant type. This is evidenced by a strongly pronounced asymmetry of the spectra exhibited in Fig. 1. Moreover, in the family of angular spectra, this asymmetry manifests itself symmetrically with respect to the almost perfect resonance curve $\rho_{\theta=50^\circ}(\theta)$ (bold curve).

It may seem that the resolution of the dependences $\rho(\lambda)$ into real components – e.g., the approximation of spectra by Gaussian functions, as was made in work [18] – is not problematic with the help of modern computer facilities. However, the extraction of components in the "pure" form from the function $\rho(\lambda)$ is interfered by the presence of one more component associated with the non-resonant reflection from the metal and glass. According to all its attributes, the spectrum of the non-resonant component in Fig. 1 should look like a curve with a definite amplitude that connects the points located beyond the examined interval, where the angular characteristics coincide. Within this interval, its magnitude depends on the experimental conditions, namely, the film thick-
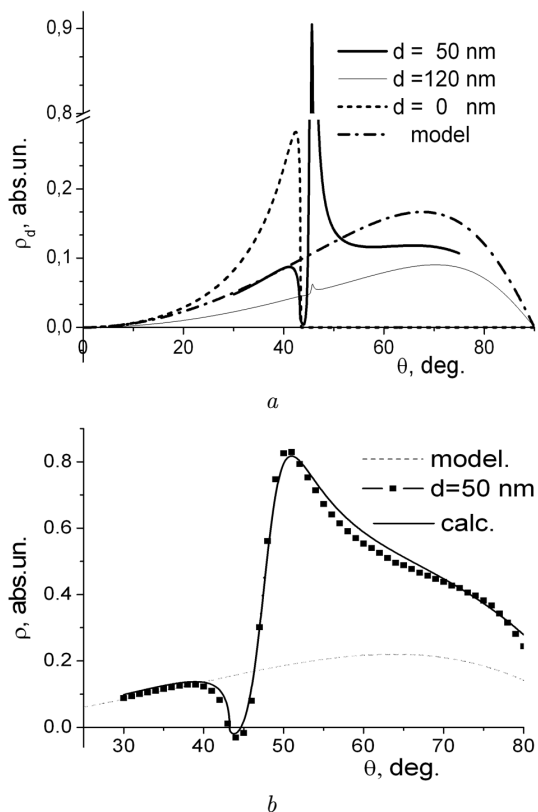
Fig. 2. (*a*) Dependences $\rho(\theta)$ at $\lambda = 632$ nm for Au films of various thicknesses and the model non-resonant component for a film with $d = 50$ nm. (*b*) The same as in panel (*b*) but for a film with $d = 50$ nm at $\lambda = 550$ nm: experimental and theoretical dependences, and its non-resonant component (dashed curve)

ness, the optical constants depending, in turn, on the film thickness and the wavelength, and the incidence angle. With all the above-mentioned in mind, it seems impossible to obtain the required dependence in a physical way or on the basis of a mathematical formalism. At the same time, the necessity in this function stems from the fact that it plays the role of the abscissa when reproducing the experimental spectrum with the use of corresponding Gaussian functions.

Therefore, we propose to solve this problem graphically. In so doing, one should take into account that the degree of validity of the result obtained will affect the adequacy of such resonance parameters as the frequency and the relaxation time of an SPR wave, as well as the reliability of its dispersion characteristic regarded as the end product of the analysis. For this purpose, we take advantage, first of all, of the

informative form of the parameter $\rho(\theta)$ characteristic owing to its analytical abilities, which was discussed above. Then, we carry out a computer simulation of the parameter basing on the fact that, as was shown in work [16] for the case of a film with the thickness $d = 50$ nm, the equation obtained on the basis of the Fresnel formulas for a three-layer system glass–metal film–air is in excellent agreement with the experimental data. The results of this procedure for the wavelength $\lambda = 632$ nm and the refractive index $N_{\text{Au}} = 0.2 + 3.6i$ [19] are depicted in Fig. 2, *a* for two extreme cases of the SPR phenomenon emergence. In one of them, when the film thickness achieved the value $d = 120$ nm, the resonance almost disappeared (solid curve). In the other case, we took $d = 0$, which corresponded to the film absence on the semicylinder surface (dashed curve). For the sake of comparison, the experimental curve obtained for the specimen thickness $d = 50$ nm, which is optimal for the SPR manifestation, is also plotted in the same figure (dash-dotted curve). One can see that the non-resonant component in the dependence $\rho_{d=50}(\theta)$ looks like the dependence $\rho_{d=120}(\theta)$, which is almost non-resonant, except for a small deviation from the monotonicity at $\theta = 45°$. In turn, the dependence $\rho_{d=50}(\theta)$ occupies an intermediate position between the characteristics obtained in the cases of a clean semicylinder and a thick metal film. Its amplitude depends on the features of reflections from both film boundaries, and the ratio between those reflection changes together with the film thickness.

From the results of computer simulation of the parameter $\rho(\theta)$, it follows that a decrease of the film thickness or the absorption index of the film (the latter is associated with a reduction of the probing radiation wavelength) is accompanied by a distortion of the monotonic dependence of the parameter $\rho(\theta)$ owing to a growth of the resonant reflection in the range of angles in a vicinity of θ_{cr}. In this case, the non-resonant component can be obtained in the form $\rho(\lambda)$ in a special manner. The essence consists in constructing the corresponding function, the amplitude values of which must be obtained from a curve that fills the resonant break in the angular dependences measured at indicated wavelengths. As such a curve, which is the closest by its form to the experimental one, the function of external reflection can be selected. While simulating this curve by an equation obtained on the basis of the Fresnel formulas, such optical parame-

ters of the film were used, at which the model curve coincided with the experimental dependence $\rho(\theta)$ at $\theta < \theta_{cr}$ and filled the resonant break. The difference between the amplitudes arising owing to the different refractive indices for radiation propagating in opposite directions, can be eliminated by fitting the coefficient until the theoretical curve coincides with the experimental one obtained at $d = 50$ nm.

The result calculated for the wavelength $\lambda = 632$ nm is shown in Fig. 2, *a* by a dash-dotted curve, which occupies an intermediate position between the curves that characterize the reflection from the metal or glass separately. In general, this curve contains the coefficient amplitudes for reflections from the metal and glass taken in the ratios that mainly depend on two parameters, the thickness and the absorption index of the film. An additional argument in favor of the curve relevance is the fact that, at the angles $\theta < \theta_{cr}$, the curve coincides with the real one, and its extreme point at $\theta > \theta_{cr}$ has the same position in the $\rho_{max}(\theta)$-coordinates as that determined by the model dependence.

The same procedure was used to plot the angular dependences $\rho(\theta)$ for certain wavelengths from the examined interval. As an example, in Fig. 2, *b*, the dependence of the parameter $\rho(\theta)$ for the different wavelength $\lambda = 550$ nm is depicted, and its comparison is made with the approximating (thin) curve and the calculated dependence (dashed curve) used as a model non-resonant function. The number of such operations was chosen from the reasons of the sufficiency of points required to plot non-resonant spectra for fixed incidence angles, which were used in Fig. 1. Then, from the angular dependences $\rho(\theta)$ obtained at various wavelengths, the corresponding ordinates of the same angles in the modeling curve were selected from the angle interval $40° < \theta < 60°$ as the coordinates of non-resonant spectra. In Fig. 3, only two of them are exhibited, which are extreme ones for the used range of angles.

The validity of the used technique can be evidenced by the fact that all non-resonant curves, by their form, resemble the experimental one $\rho_{d=40}(\theta)$ from Fig. 1, from which the attributes of the resonant reflection are absent. The other non-resonant curves, which were not presented in order to simplify the illustration, fill the interval between two shown curves in a logic sequence. Concerning a resonance-like dip at $\lambda \approx 500$ nm observed in all obtained curves, it
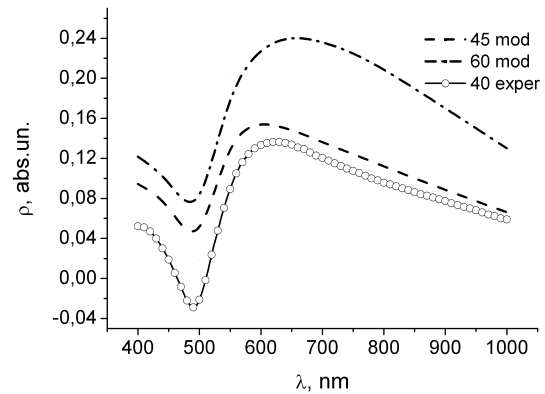

Fig. 3. Spectral dependences of the non-resonance component of the parameter $\rho(\theta)$ obtained at the measurement at the incidence angle $\theta = 40°$ and the model curves calculated for the angles $\theta = 45°$ and $60°$
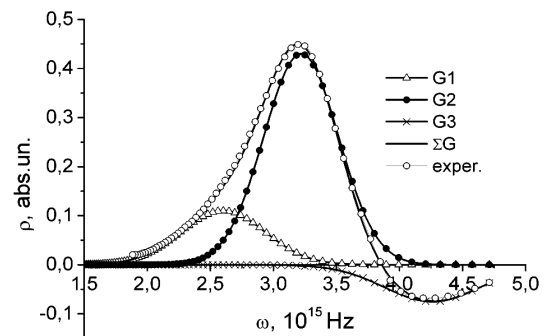

Fig. 4. An example of the approximation of one of the experimental dependences in Fig. 1 measured at $\theta = 47°$ using Gaussian functions

formally originates from a cusp located at this wavelength in the dispersion of the refractive index of the Au film. In this connection, the approach of the amplitudes of the reflection coefficient curves $R_s^2(\theta)$ and $R_p^2(\theta)$ to each other, which is testified by the dips in the curves shown in Fig. 3, may have a physical origin, the establishment of which goes beyond the scope of this work.

After the non-resonant dependences have been subtracted from the corresponding experimental ones (Fig. 1), the procedure of approximating the obtained result by Gaussian functions does not cause difficulties. As an illustration, the result of the resolution of the spectrum obtained at the incidence angle $\theta = 47°$ into its components is demonstrated in Fig. 4. Two conclusions follow from this figure. First, the almost perfect filling of the experimental dependence by the
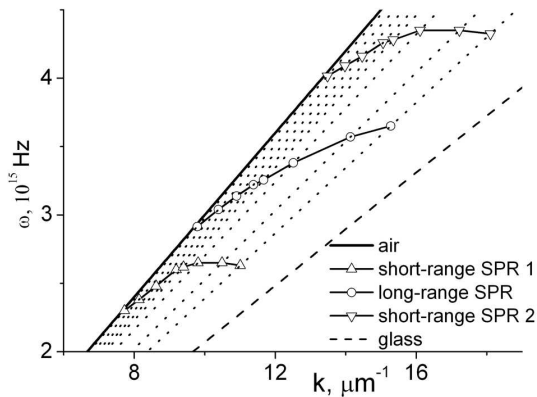
Fig. 5. Dispersion characteristics $\omega(k)$ of the SPR in an Au film with $d = 50$ nm
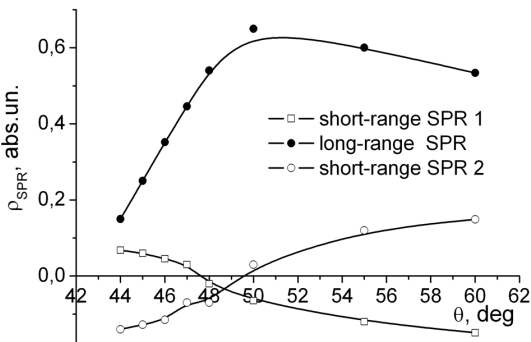

Fig. 6. Dependences of the amplitudes of Gaussian-like components that approximate the normalized ρ_{SPR} on the light incidence angle

total approximating function is observed (the corresponding curves merge together), which testifies to the reliability of the result obtained. Second, the perfect filling turns out possible only if three components are taken into account. Therefore, the frequency and amplitude characteristics were obtained by resolving the normalized dependences $\rho(\lambda)$ into Gaussian components.

Before discussing the interpretation of the components, it is pertinent to note that the three-layer structure used here was considered earlier [20], by solving the Maxwell equations. The cited authors obtained the waveguide modes that arise at two metal–insulator interfaces adjacent to a metal film. Those modes were called symmetric (s-mode) and asymmetric (α-mode) on the grounds that the electric field of α-mode has the inverted phase at the internal surface of a metal film. The authors of work

[20] had some reasons to consider that those solutions can be extended to describe the field distributions that arise in the case of the resonance excitation at definite indicated interfaces. This procedure is especially possible in the case of the SPR observation in the Kretschmann geometry [21] used in this work, in which the phase asymmetry of the α-mode is combined with the profile asymmetry of the excited surface polariton wave field. When radiation from the glass prism with total internal reflection falls at an oblique angle on a metal film, the energy is mainly concentrated near the interface between the metal and the insulator with a lower refractive index (this is the long-range mode). The short-range mode with a lower energy is concentrated near the interface between the metal and the insulator with a higher refractive index, i.e. at the internal film surface. It is the latter wave mode existing in the form of a wave excited at the internal film surface that can change its phase with respect to the fast mode. Such a phase behavior may be induced by the change in the sign of the electric polarization at the front film surface in the case where the fields of the incident wave and the wave reflected from the back surface are superimposed on this surface. A real basis for such an evolution is the spectrally dependent variation of the absorption coefficient (index) at a constant film thickness, or at a film thickness at a fixed radiation wavelength.

The results of the spectral analysis shown in Fig. 5 in the form of dispersion characteristics $\omega(k_{SPR})$ qualitatively confirm our theoretical conclusions made above. These characteristics were plotted by connecting separate points obtained using the described technique and located on the corresponding light lines $k_{SPR} = \sqrt{\varepsilon_g} \sin\theta$, where ε_g is the glass dielectric permittivity. As follows from the figure, the main waveguide mode (the long-range SPR), or the surface plasmon–polariton wave, spans the frequency interval $\omega = (3 \div 4) \times 10^{15}$ Hz. The SPR component excited at the internal surface of the gold film is called a short-range waveguide mode [20] (the short-range SPR) and occupies two frequency intervals located above and below the frequencies of the main SPR.

In Fig. 6, the dependences of the amplitudes of all three components on the light incidence angle are exhibited. They allow each of two variants of the short-range mode to be classed as symmetric, with their sign coinciding with that of the main mode; and

the third one as asymmetric. The figure also demonstrates a more exact, in comparison with Fig. 1, value of the reflection symmetry angle equal to $\theta = 49°$.

3. Conclusions

In accordance with the predictions made in work [20] and with the use of the modulation polarimetry technique, various components of the resonant interaction between electromagnetic radiation and the electron-ion system of the substance was revealed in such a simple medium as a nano-sized film of the homogeneous metal. For this purpose, however, we had to develop a method to analyze such spectral characteristic of the SPR as the polarization difference parameter $\rho(\lambda)$. The necessity of this procedure was dictated by the form asymmetry revealed for the experimental characteristics of the parameter $\rho(\lambda)$. Moreover, this asymmetry is characterized by the reflection inversion with respect to the spectral characteristic for the light incidence angle $\theta = 49°$, as well as by the inversion of the parameter $\rho(\lambda)$ sign for the short-range SPR modes.

An obstacle for the resolution of spectra into their components was the presence of non-resonant components in their content, the magnitudes of which were indefinitely distributed over the spectrum. The procedure of determining their spectra, which consists in simulating the angular characteristics of the polarization difference $\rho(\theta) = R_s^2 - R_p^2$ in the form of monotonic dependences that fill the resonant break in the analogous function of the real specimen, was elaborated. Then the set of amplitudes of the coefficients $\rho(\theta)$ at definite wavelengths from the investigated spectral range was used to calculate the spectra of non-resonant components at corresponding angles. After subtracting each of them from the corresponding spectrum $\rho_\theta(\lambda)$, the normalized spectral dependence of the resonant parameter $\rho_{\text{SPR}}(\lambda)$ was obtained. An almost perfect coincidence of the experimental $\rho_{\text{SPR}}(\lambda)$ curve with the approximating sum of Gaussian functions testifies to the validity of the proposed procedure. Moreover, the resolution of the normalized spectral dependence $\rho_{\text{SPR}}(\lambda)$ into components allowed us to register the long- and short-range wave modes described in work [22] and identify them as polariton waves at the external and internal, respectively, surfaces of a metal film. In addition, the transition of the

symmetric state into the asymmetric one was detected in the spectral and angular characteristics of the short-wave mode measured at a fixed angle of light incidence for the specimen 50 nm in thickness.

1. *Surface Polaritons: Electromagnetic Waves at Surfaces and Interfaces,* edited by V.M. Agranovich and D.L. Mills (North-Holland, Amsterdam, 1982).

2. N.L. Dmitruk, V.G. Litovchenko, and V.L. Strizhevskii, *Surface Polaritons in Semiconductors and Insulators* (Naukova Dumka, Kyiv, 1989) (in Russian).

3. H. Raether, *Surface Plasmons on Smooth and Rough Surfaces and on Gratings* (Springer, Berlin, 1988).

4. U. Kreibig and M. Vollmer, *Optical Properties of Metal Clusters* (Springer, Berlin, 1995).

5. S. Kawata and H. Masuhara, *Nanoplasmonics* (Elsevier, Amsterdam, 2006).

6. S.A. Maier, *Plasmonics: Fundamentals and Applications* (Springer, New York, 2007).

7. D. Woolf, M. Loncar, and F. Capasso, Opt. Express **17**, 22 (2009).

8. L.A. Golovan', V.Yu. Timoshenko, and P.K. Kashkarov, Usp. Fiz. Nauk **177**, 6 (2007).

9. V.V. Klimov, Usp. Fiz. Nauk **178**, 8 (2008).

10. N.G. Khlebtsov, Kvant. Elektron. **38**, 6 (2008).

11. I.D. Voitovich and V.M. Korsunskii, *Sensor Controls on the Basis of Plasmon Resonance: Principles, Technologies, Applications.* (Stal', Kyiv, 2011) (in Russian).

12. V.S. Grinevich, L.M. Filevska, I.E. Matyash, L.S. Maximenko, O.N. Mischuk, S.P. Rudenko, B.K. Serdega, V.A. Smyntyna, and B. Ulug, Thin Solid Films **522**, 452 (2012).

13. L.I. Berezhinskii, O.S. Litvin, L.S. Maksimenko, I.E. Matyash, S.P. Rudenko, and B.K.Serdega, Opt. Spektrosk. **107**, 2 (2009).

14. B.K. Serdega, S.P. Rudenko, L.S. Maksimenko, and I.E. Matyash, in: *Polarimetric Detection, Characterization, and Remote Sensing* (Springer, Berlin, 2011).

15. L.I. Berezhinskii, L.S. Maksimenko, I.E. Matyash, S.P. Rudenko, and B.K.Serdega, Opt. Spektrosk. **105**, 2 (2008).

16. A. Gerrard and J.M. Burch, *Introduction to Matrix Methods in Optics* (Wiley, London, 1975).

17. S.N. Jasperson and S.E. Schnatterly, Rev. Sci. Instrum. **40**, 6 (1969).

18. D.A. Grin'ko, Yu.M. Barabash, L.S. Maksimenko, I.E. Matyash,, O.N. Mishchuk, S.P. Rudenko, and B.K. Serdega, Fiz. Tverd. Tela **54**, 11 (2012).

19. H. Piller, in *Handbook of Optical Constants of Solids*, edited by E.D. Palik (Elsevier, Amsterdam, 1997), Vol. II, p. 637.

20. J.J. Burke and G.I. Stegeman, Phys. Rev. A **33**, 8 (1986).

21. E. Kretschmann, Z. Phys. **241**, 313 (1971).

22. H. Yoon, S.A. Maier, D.C. Bradley, and P.N. Stavrinou, Opt. Mater. Express **1**, 6 (2011).

Л.С. Максименко, І.Є. Матяш, О.М. Міщук,
С.П. Руденко, Б.К. Сердега, М.О. Стеценко

СПЕКТРАЛЬНИЙ АНАЛІЗ ПОЛЯРИЗАЦІЙНИХ
ХАРАКТЕРИСТИК ПОВЕРХНЕВОГО ПЛАЗМОННОГО
РЕЗОНАНСУ В НАНОРОЗМІРНІЙ ПЛІВЦІ ЗОЛОТА

Р е з ю м е

Методом внутрішнього відбиття із застосуванням техніки модуляційної поляриметрії досліджено поляризаційні властивості поверхневого плазмонного резонансу в нанорозмірній плівці золота, що була виготовлена термічним випаровуванням. Виміряно спектральні і кутові характеристики коефіцієнтів відбиття лінійно поляризованих випромінювань при стаціонарних азимутах поля хвилі паралельно R_p^2 та перпендикулярно R_s^2 площині падіння, а також характеристики їх поляризаційної різниці $\rho = R_\mathrm{s}^2 - R_\mathrm{p}^2$, що є продуктом модуляційної методики. Виявлено яскраву асиметрію профілю в спектрах параметра $\rho(\lambda)$. Вироблено методику визначення величини нерезонансної компоненти в спектрах $\rho(\lambda)$, з урахуванням якої проведено їх апроксимацію функціями Гауса. В отриманих характеристиках $\rho_\mathrm{SPR}(\lambda)$ виявлено три резонансні компоненти. Запропоновано їх інтерпретацію, яка ґрунтується на опублікованій раніше теоретичній моделі хвилеводних мод на обох поверхнях плівки. Визначено параметри резонансів, на підставі яких побудовано дисперсійні залежності.